# Relationship between plaque development and local hemodynamics in coronary arteries

Andreas Wahle,[a] John J. Lopez,[d] Mark E. Olszewski,[a] Sarah C. Vigmostad,[b] Kathleen C. Braddy,[c] Theresa M. H. Brennan,[c] Syed W. Bokhari,[d] J. Gray Bennett,[d] Elizabeth M. Holper,[d] James D. Rossen,[c] Krishnan B. Chandran,[b] and Milan Sonka[a]

The University of Iowa, [a]Department of Electrical and Computer Engineering, [b]Department of Biomedical Engineering, and [c]Department of Internal Medicine, Iowa City, IA 52242, USA

[d]The University of Chicago, Department of Medicine, Chicago, IL 60637, USA

## ABSTRACT

The mechanisms of plaque development in coronary arteries are not yet completely understood. Vessel geometry influences the local hemodynamics within a vessel, and the resulting wall shear stress in turn influences plaque development. Previously, we showed in-vivo that plaque tends to accumulate more on the inner curvature of a vessel than on its outer curvature. While vessel curvature is preserved during plaque progression, the local wall shear stresses change with lumen narrowing. The aim of this study was to test how the hypothesis that locations of low wall shear stress coincide with circumferentially larger plaque accumulation depends on vascular remodeling with or without lumen narrowing. We have analyzed 39 in-vivo intravascular-ultrasound pullbacks, for which geometrically accurate 3-D models were obtained by fusion with x-ray angiography. Distorting subsegments (branches, calcifications, stents) were discarded, and the relative number of vessel locations was determined within a 10–40% area-stenosis range. This range corresponds to *compensatory enlargement* (outward or positive vessel remodeling), but not yet lumen narrowing, and these vessel segments were a focus of our study. For each segment, we determined the relative number of vessel locations for which circumferentially low wall shear stress coincided with larger plaque thickness and vice versa. The inverse association between wall shear stress and plaque thickness was significantly more pronounced ($p<0.005$) in vessel cross sections exhibiting compensatory enlargement without luminal narrowing than when the full spectrum of vessel stenosis severity was considered. Thus, the hypothesis is supported more in subsegments with less developed disease.

**Keywords:** Coronary arteries, computational hemodynamics, plaque progression, intravascular ultrasound, x-ray angiography, 3-D multimodality fusion

## 1. INTRODUCTION

Coronary atherosclerosis starts early in life and is a major cause of death in industrialized countries. As shown in Fig. 1(a)–(c), the earliest stage of plaque development is intimal thickening.[1,2] However, the lumen size remains constant through the early atherosclerosis process due to *compensatory enlargement*. Luminal narrowing, demonstrated as an angiographically visible stenosis, generally occurs after the plaque area exceeds about 40% of the cross-sectional vessel area.[3] Obstructive stenoses, when they cause symptoms or impairment of myocardial function, are often treated by percutaneous transluminal coronary angioplasty (PTCA) and subsequent stenting to restore the lumen, illustrated in Fig. 1(d). Intravascular ultrasound (IVUS) is able to visualize plaque development and treatment results,[4] as shown in Fig. 1(e). Previous studies have linked plaque development with low wall shear stress.[5] Thus, the identification of areas of initially low wall shear stress and the evaluation of the plaque distribution is of major interest, especially given the capabilities of IVUS to image plaque. As is typical for coronary IVUS studies, all subjects imaged had clinically indicated cardiac catheterization. It is imprudent to perform IVUS imaging in patients with healthy or minimally diseased coronary vessels. Consequently, the enrolled subjects invariably suffered from advanced coronary artery disease. As such, the relationships we observed were between an already substantially altered coronary morphology and the related altered hemodynamic shear

E-mail: <andreas-wahle@uiowa.edu>; http://www.engineering.uiowa.edu/~awahle; Fax: +1-319-335-6028

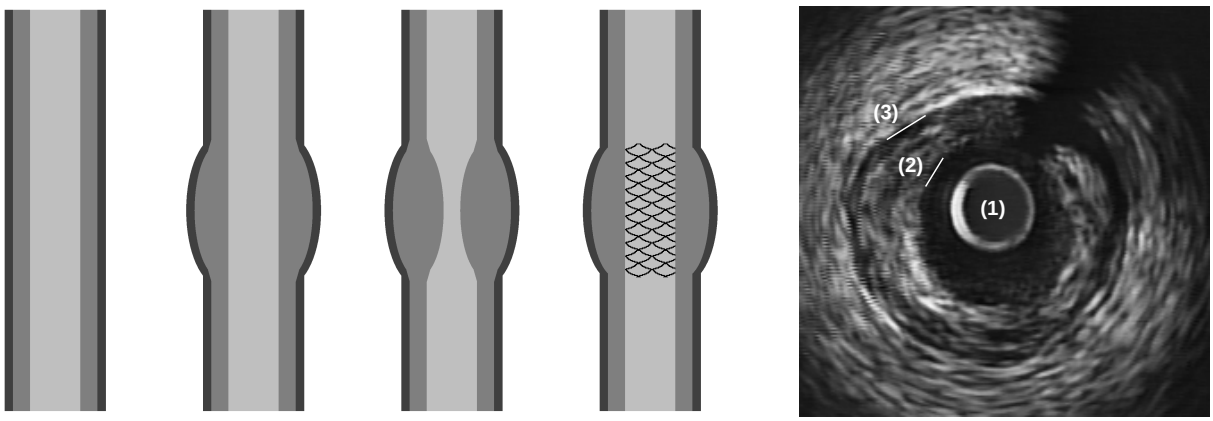


**Figure 1.** Development of atherosclerotic plaque: lumen — light gray, plaque/intima — mid gray, media — dark gray; (a) vessel without any stenosis; (b) compensatory enlargement; (c) luminal narrowing; (d) after treatment with PTCA and stenting; (e) IVUS image with (1) catheter, (2) lumen/plaque, and (3) media/adventitia borders.

stress conditions. It has been shown that, with extensive luminal narrowing, the inverse relationship between plaque thickness and wall shear stress is no longer preserved.[6] In addition to this phenomenon, we were also interested in the notion that hemodynamic shear stress plays a role in the onset of coronary disease. In contrast to wall shear stress, vascular geometry (curvature) is not changed by the course of the disease and thus can serve as a surrogate of the hemodynamic conditions prior to atherosclerotic disease development. Therefore, the relationship between vessel curvature and plaque distribution was studied as well as the relationship between wall shear stress and plaque distribution with special consideration of vascular remodeling.

## 2. METHODS

### 2.1. Fusion between x-ray angiography and intravascular ultrasound

We have developed a comprehensive system that generates geometrically correct 3-D and/or 4-D (i.e., 3-D plus time) reconstructions of coronary arteries and computers corresponding quantitative indices of coronary lumen and wall morphology. The reconstructions serve as input for hemodynamic analyses and allow for interactive visualization.[4, 7–9] A flowchart outlining the system is given in Fig. 2. In brief, the vessel geometry is obtained from biplane (or a pair of single-plane) x-ray angiographic projections, whereas the cross-sectional information is retrieved from IVUS. Thus, the resulting model accurately reflects the curvature and torsion of the vessel as well as any accumulated plaque. The angiography and IVUS data are retrospectively ECG-gated and segmented. Fusion leads to the 3-D/4-D *plain model*, consisting of the luminal and adventitial contours oriented relative to the IVUS catheter. After tetrahedral meshing, this model is suitable for hemodynamic analyses. Following resampling orthogonal to the vessel centerline, morphologic analyses are performed. The quantitative results *annotate* the resampled contour model, which is subsequently used for visualization and further analyses. Our system utilizes conventional PC hardware and widely available software tools. Standardized storage formats for parameters and contour lists have been adopted to ensure proper interfacing between our fusion system and commercially available analysis software packages and to enhance data sharing and collaboration.[8]

### 2.2. Segmentation of IVUS image data

While many components of the fusion system perform to full satisfaction, several challenges remain. One of them is the segmentation of the IVUS data. It is well known that IVUS images contain artifacts from various sources, thus requiring the design of cost functions that incorporate a-priori knowledge of regional and border properties to robustly determine the optimum contours. The cost function employed in our graph-based IVUS segmentation method combines three major groups of features: (a) image data terms such as edge detectors and intensity patterns; (b) physics-based terms that distinguish different tissue types based on their Rayleigh

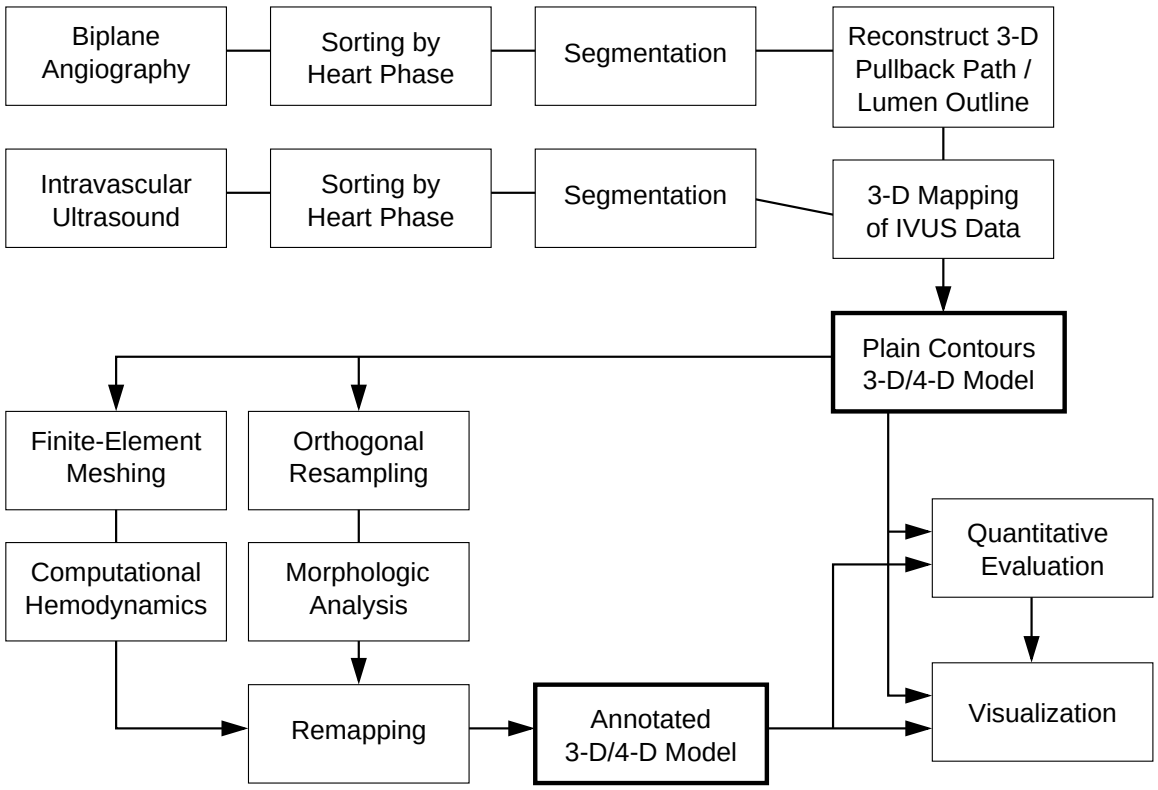


**Figure 2.** Processing of the data from acquisition over segmentation to the generation of the *plain* model, followed by quantitative analyses used to *annotate* the 3-D/4-D model.

distribution patterns[10,11]; and (c) border probabilities based on expert tracings. A scoring system is employed to evaluate these feature classes in each image to be analyzed, and the borders are found using a multiresolution approach that mimics human vision.[12,13]

### 2.3. Quantitative indices of vessel morphology and hemodynamics

The reconstructed vascular model provides 3-D locations for 72 circumferential vertices on both lumen/plaque and media/adventitia contours, radially oriented with respect to the vessel centerline. This allows a straightforward determination of the plaque thickness at each location, as well as volumetric measurements over any given subsegment of the vessel.[14] In order to determine local curvature magnitude and direction, computational geometry was employed. To distinguish between locations of "inner" vs. "outer" curvature on the circumference of the vessel, a new scheme was introduced that weights the curvature magnitude by an index of the circumferential position of each element.[15,16] Blood flow through the coronary arteries was simulated using *computational fluid dynamics* (CFD) methodology. Tetrahedral meshing of the lumen using commercially available meshing software provides an unstructured grid for simulations with U$^2$RANS, a CFD software developed at The University of Iowa.[17,18] Positive and negative wall shear stress values are determined at each circumferential lumen location and mapped onto the 3-D model.

### 2.4. Classifying circumferential plaque distribution, curvature, and wall shear stress

Each of the 72 circumferential locations in each vessel cross section was categorized with respect to its relative plaque thickness (above or below average for this cross section), its location relative to the local vessel curvature (inner or outer curvature), and its wall shear stress (above or below cross-sectional average). In this way, eight different "regions" resulted. A ninth "neutral" region included those areas of curvature magnitude below a certain threshold that were eliminated from further analysis to avoid distortion of the results by noise. The following two studies correlate independently plaque distribution with curvature and wall shear stress.

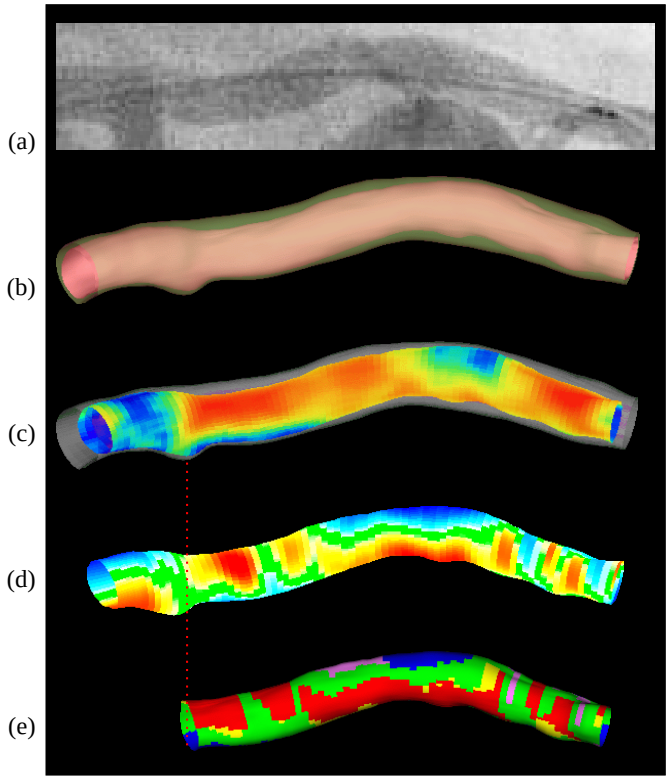


**Figure 3.** Plaque thickness vs. curvature:

(a) angiogram of a left anterior descending artery with the IVUS catheter inserted;

(b) 3-D model with lumen and adventitia borders from fusion, where the volume between the red and green surfaces represents the vessel wall;

(c) plaque-thickness annotation derived from the model shown in (b), where blue color indicates low and red color high wall thickness;

(d) curvature-index annotation derived from (b), blue color marks "outer" and red "inner" curvature;

(e) after classification into regions correlating the data from (c) and (d), with the branch segment removed from analysis; see text for the definition of the regions.

please refer to the electronic version for this figure in color

## 3. STUDIES AND RESULTS

### 3.1. Relation between plaque distribution and vessel curvature

#### 3.1.1. The plaque/curvature index

To verify the observation that plaque tends to accumulate at the inner bend of the curvature rather than at the outer bend of the curvature, the relative amount $r_{PC}$ of regions where inner curvature coincides with above-average plaque accumulation, or outer curvature coincides with below-average plaque accumulation, was determined in a set of 53 vessels. Preliminary results and methodology were reported previously.[15,16] The ratio $r_{PC}$ represents a "plaque/curvature index" with a value $r_{PC}$>0.5 indicating that more plaque has accumulated along the inner curvature as compared to the outer curvature, thus supporting the hypothesis. As an example, Fig. 3(c) shows a color-coded plaque-thickness distribution in a geometrically correct 3-D representation, with red indicating high and blue indicating low plaque thickness, normalized over the entire vessel segment. As described above, a curvature index was determined for each circumferential location on the contour. Fig. 3(d) shows the color-coded curvature-index distribution, with red indicating inner curvature and blue indicating outer curvature. Four regions were defined, as depicted in Fig. 3(e): $R_{ai}$ (red), $R_{ao}$ (magenta), $R_{bi}$ (yellow), and $R_{bo}$ (blue). These regions represent pairs distinguishing circumferentially considered "above-average" plaque thickness ($a$) from "below-average" plaque thickness ($b$), coinciding with either "inner curvature" ($i$) or "outer curvature" ($o$) of the vessel wall. Thus, the plaque/curvature index was defined as

$$r_{PC} = \frac{\|R_{ai} + R_{bo}\|}{\|R_{ai} + R_{bo} + R_{ao} + R_{bi}\|} \tag{1}$$

#### 3.1.2. Results by curvature threshold and vessel type

The results are depicted in Fig. 4 and Tab. 1. Twelve different threshold values were empirically selected ranging from 2.31 to 22.94°/cm, resulting in 10.1–78.0% of circumferential locations being assigned to the neutral region

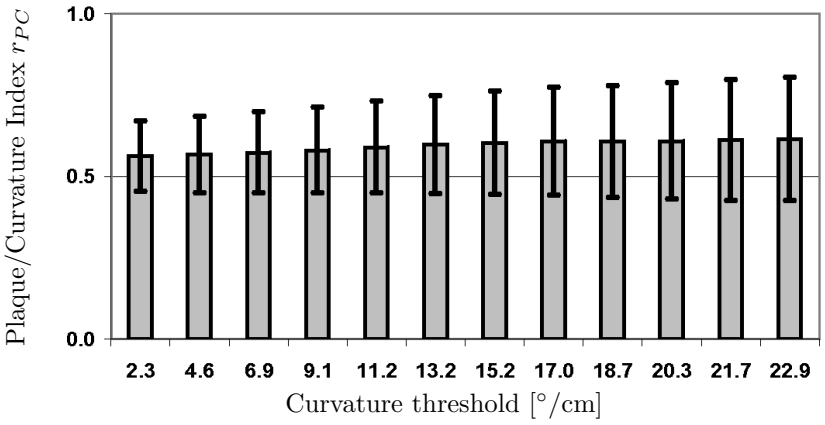


**Figure 4.** Results from 53 analyzed vessels, means and standard deviations per curvature threshold, with $r_{PC}$>0.5 indicating that our guiding hypothesis was satisfied.

| | $r_{PC}>0.5$ for $n$ thresholds | | | | |
|---|---|---|---|---|---|
| *Vessel* | 12 | ≥6 | ≥1 | =0 | |
| LAD | 16 | 2 | 1 | 1 | *20* |
| RCA | 8 | 4 | 1 | 7 | *20* |
| LCX | 8 | 1 | 0 | 4 | *13* |
| | *32* | *7* | *2* | *12* | *53* |

**Table 1.** Results from Fig. 4 by curvature threshold and vessel, with $r_{PC}$>0.5 satisfied for all (12), at least half (≥6), at least one (≥1), or none (=0) of the curvature thresholds.

$R_n$ (green), also included in Fig. 3(e). The chart shows that the average $r_{PC}$ over all 53 vessels increases steadily with increase of the curvature threshold. With increasing threshold, more regions of low curvature are included into $R_n$. Consequently, the proportion of higher curvature regions included in the calculation of $r_{PC}$ is increased. Since regions of higher curvature support the hypothesis stronger, a respective increase of $r_{PC}$ with the threshold is seen. The increase in standard deviation of $r_{PC}$ prompted us to categorize the results by vessel. Overall, almost two thirds of the vessels satisfied $r_{PC}$>0.5 for *all* of the 12 thresholds. The hypothesis was most strongly supported in the left anterior descending (LAD) arteries, where 90% of the vessels showed $r_{PC}$>0.5 for all or at least half of the thresholds. Since the right coronary (RCA) and left circumflex (LCX) arteries tend to be more curved and tortuous than the LAD, the less supportive results may be caused by the more complex flow patterns that can no longer be explained by the curved-tube model.

### 3.1.3. Impact of PTCA and stenting

Stenting may have a substantial impact on the outcome of the plaque/curvature index $r_{PC}$. In several of the vessels analyzed, a below-threshold value of $r_{PC}$ ($r_{PC}$<0.5) was determined when all segments were included and only branch locations were excluded. After also excluding known regions of intervention and stenting, $r_{PC}$>0.5 was reached, frequently showing the increase of $r_{PC}$ with the increase in curvature threshold (Figs. 5, 6). This contradicts our initially reported findings in a smaller subset of patients[16] in which the plaque/curvature index $r_{PC}$ was not significantly different whether or not stented regions were included in the analysis. Our new results rather suggest that substantial disease and stenting *may* have a distorting impact on the relation between vessel geometry and plaque distribution. Thus, further statistical analysis will be performed as data from additional subjects become available.

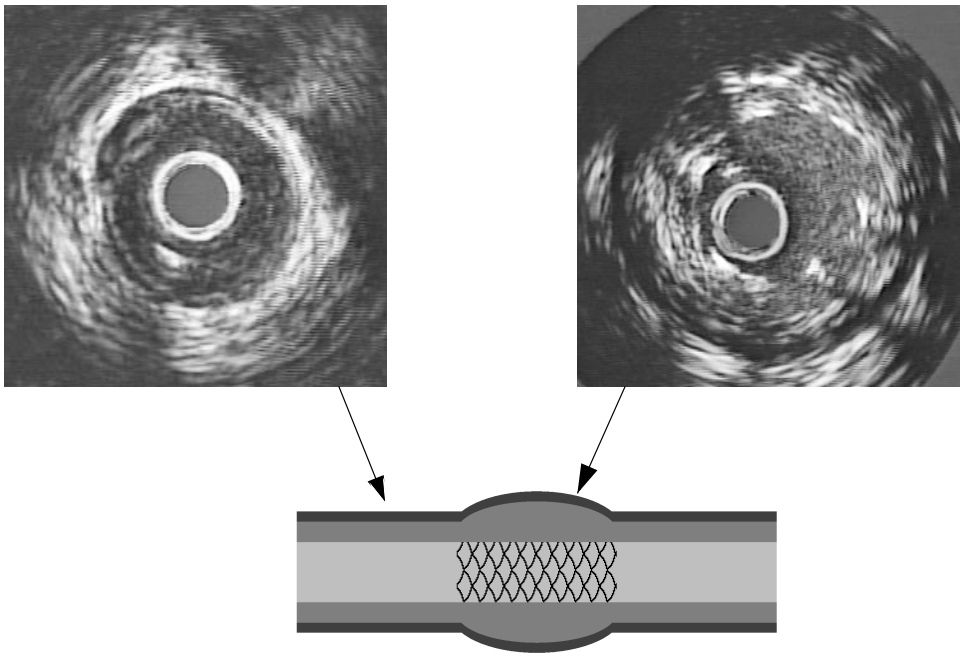

**Figure 5.** IVUS frames of an untreated vessel segment with slight stenosis and after stent placement at a location with heavy disease.

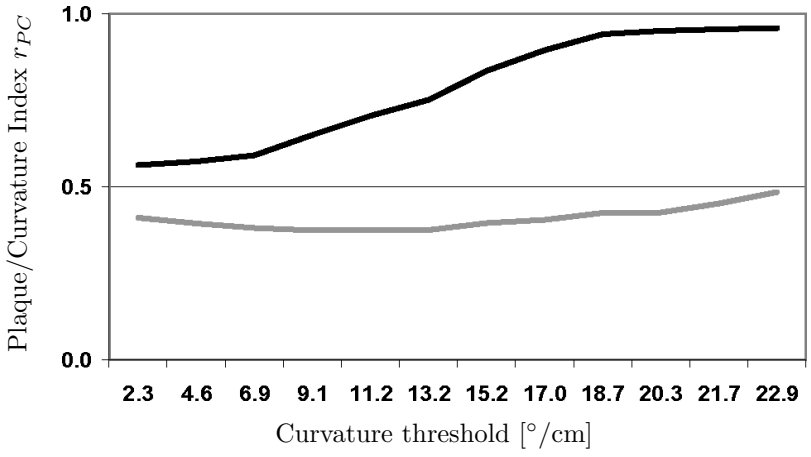


**Figure 6.** Index $r_{PC}$ for the vessel shown in Fig. 5 over the full vessel (gray) and with stented subsegments excluded (black); the hypothesis is only satisfied after exclusion of the diseased segment as compared to the overall vessel.

### 3.2. Relation between plaque distribution and wall shear stress

While disease progression and stenting impact the curvature/plaque relationship to some extent, an even more substantial effect can be expected on the wall shear stress distribution. The distribution is substantially altered when the limits of positive remodeling are reached.[6] Thus, the vessel subsegments for which the area stenosis is between 10% and 40% are of specific interest. This range corresponds to compensatory enlargement as identified by Glagov et al.[3] Consequently, we concentrated on whether and how significantly the correlation improves once vessel segments of certain properties are excluded from the analysis. In this way, indirect evidence of which local conditions favor the underlying hypothesis of below-average wall shear stress inducing above-average plaque thickness was sought.

#### 3.2.1. The plaque/wall-shear-stress index

39 vessels (a subset of Section 3.1, since some parameters were not available for vessels received from collaborating sites) were analyzed. The data was smoothed with a moving 45°-wedge over 5 frames to limit the impact of local noise. The analyses were performed in 4 increasingly restrictive subsets of data. First, the relative amount $r_{PW}$ of elements for which circumferentially above-average plaque thickness coincides with below-average wall shear stress (and vice versa) was determined for each vessel segment – similar to the plaque-thickness/curvature study. By replacing "inner curvature" ($i$) with "lower-than-average wall shear stress" ($l$) and "outer curvature" ($o$) with "higher-than-average wall shear stress" ($h$) in Eq. (1),

$$r_{PW} = \frac{\|R_{al} + R_{bh}\|}{\|R_{al} + R_{bh} + R_{ah} + R_{bl}\|} \tag{2}$$

results as definition for the plaque/wall-shear-stress index.

#### 3.2.2. Automated grouping of vessels and segments by disease severity

The collection of vessels and their associated plaque/wall-shear-stress indices create Set #1. Next, all vessel subsegments that included vessel branching areas, stents, or regions of dense calcification were excluded, forming Set #2. Within Set #2, percent-area stenosis was determined for each frame following Glagov's definition, which does not require the presence of a normal reference segment.[3] Specifically, the combined plaque and wall area over the total cross-sectional vessel area was calculated. Set #3 consisted of all such vessels from Set #2 for which the percent-area stenosis was in the range of 10–40% in at least 35% of the non-excluded vessel segments. The 35% threshold has been determined empirically by clustering of the plaque/wall-shear-stress index distribution and may need to be slightly adjusted when more data from additional subjects becomes available for analysis. Set #3 consisted of 24 vessels satisfying this criterion. In each vessel, the segments of Sets #2 and #3 that were within the 10–40% range of area stenosis formed Subsets #2a and #3a. An illustration for the definition of these sets is shown in Fig. 7.

#### 3.2.3. Changes in plaque/wall-shear-stress indices on advanced-disease segment exclusion

If the hypothesis is correct and observable in regions where severe luminal narrowing is not present, the vessels in Subsets #2a and #3a should provide higher $r_{PW}$ ratios than the corresponding vessels in Sets #2 and #3. Therefore, we determined factors $g_{PW}$ quantifying the change $g_{PW\{2\}} = r_{PW\{2a\}}/r_{PW\{2\}}$ for all vessels and $g_{PW\{3\}} = r_{PW\{3a\}}/r_{PW\{3\}}$ for vessels with the minimum of 35% of frames within the 10–40% area-stenosis range. Note that the $g_{PW\{x\}}$ represent the differences in hypothesis validity. Consequently, $g_{PW\{x\}}>1$ suggests a case for which the hypothesis is more strongly supported in those segments of vessel $x$ with compensatory enlargement as compared to those with lumen narrowing. The analysis rationale is to determine: (1) whether applying the hypothesis test on the subset of segments defined in Set #2a (10–40% stenosis) increases the validity of the hypothesis compared to the Set #2; and, (2) whether applying the hypothesis test on Set #3a (10–40% stenosis in vessels with ≥35% of the wall within this range) increases the hypothesis validity compared to the Set #3 (≥35% of the wall within the 10–40% stenosis range).

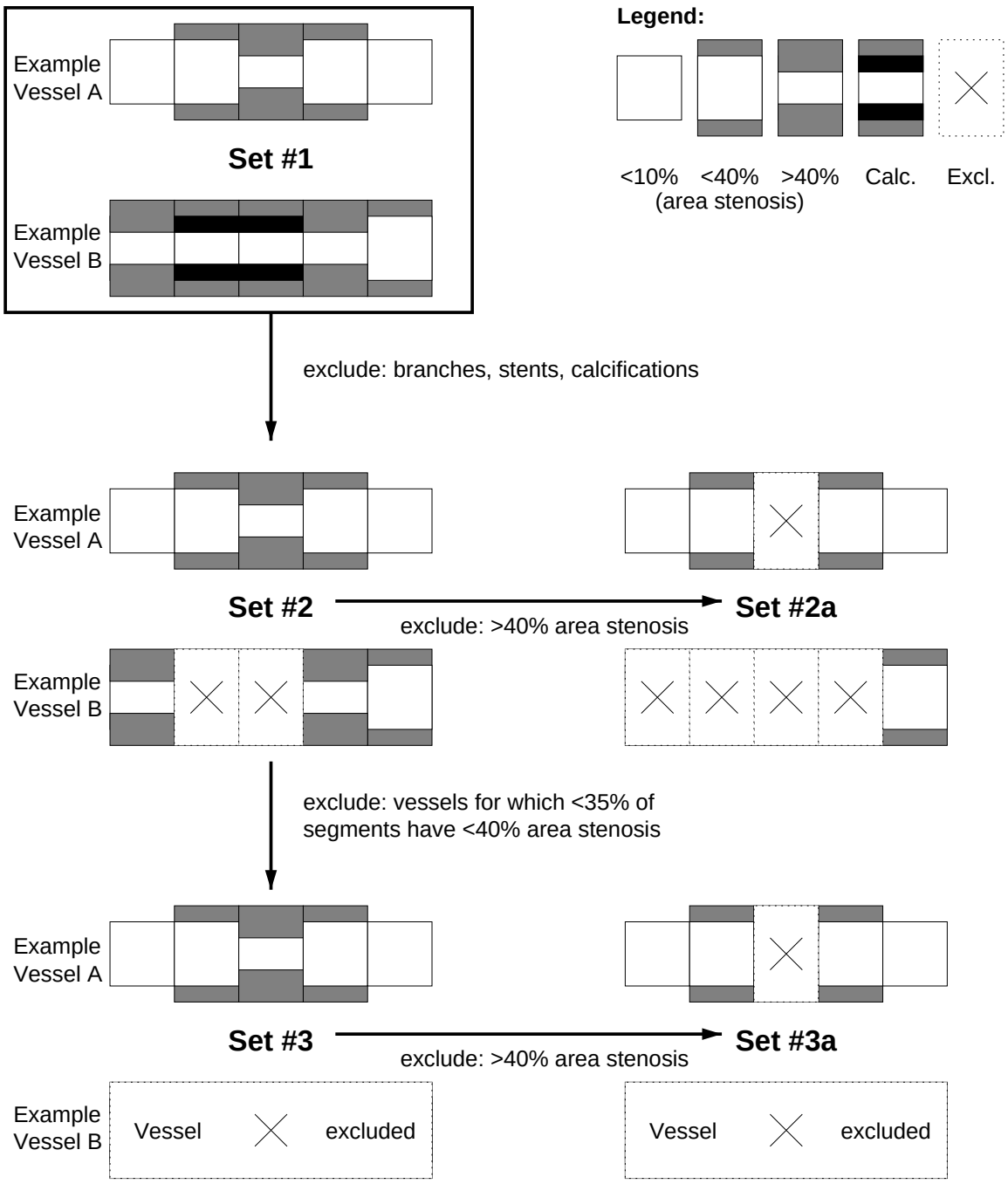


**Figure 7.** Example for the definition of the sets: Vessel A shows only minor disease, whereas Vessel B is subject to advanced atherosclerosis; both form Set #1. For Vessel A, all subsegments are retained when proceeding to Set #2, whereas two subsegments of Vessel B were discarded due to calcifications. All subsegments outside the 10–40% area stenosis range are removed from Set #2 to create Set #2a, thus discarding 1 subsegment from Vessel A and 2 subsegments from Vessel B. Only Vessel A proceeds from Set #2 to Set #3, since less than 35% of Vessel B are within the 10–40% area stenosis range. For Vessel A, (in analogy to the step from Set #2 to Set #2a) the center segment is discarded from Set #3 to Set #3a.

### 3.2.4. Results by disease-severity groups

For Set #2, 23 vessels (59.0% of 39) showed an improvement in hypothesis validity. For 2 vessels (5.1%), the hypothesis validity did not change. In 14 vessels (35.9%), the hypothesis validity decreased. In Set #3, 18 vessels (75.0% of 24) demonstrated a hypothesis validity improvement, while no change was observed in 2 vessels (8.3%), and validity decreased in 4 (16.7%) vessels. The difference in hypothesis validity (thus, the respective $g_{PW\{2\}}$ and $g_{PW\{3\}}$ values) was significant between Sets #3 and #3a ($p<0.005$), whereas it was not significant between Sets #2 and #2a ($p>0.4$). The average improvement of the $r_{PW}$ ratios in Set #3a over Set #3 was 4.9%. Interestingly, all vessels in Set #3 for which $r_{PW\{3\}}>0.54$ ($n=8$) showed a $g_{PW\{x\}}>1$ with an average improvement of 9.0%. This suggests that vessels with a relatively high applicability of the hypothesis, thus primarily in the early stages of atherosclerosis, improve even more when the analysis is restricted to areas of compensatory enlargement.

## 4. CONCLUSIONS

In this study, we have confirmed the observation that plaque tends to form at the inner curvature of the vessel wall and that plaque thickness is related to curvature in a larger set of in-vivo patient data. Our findings suggest that low wall shear stress, which is typically associated with inner vessel curvature locations, likely contributes to the *initial* formation of atherosclerotic plaque in the early stages of the disease in human coronary arteries. However, the wall shear stress distribution is altered when compensatory enlargement ceases and the lumen narrows. We have demonstrated that the hypothesis of above-average plaque thickness being associated with below-average wall shear stress is more strongly supported in the *early* stages of atherosclerosis as compared with the *later* stages of disease progression.

## ACKNOWLEDGMENTS

This work was supported in part by grant R01 HL63373 of the National Heart Lung and Blood Institute at the National Institutes of Health, Bethesda MD. The authors would like to thank Dr. Rubén Medina, Universidad de Los Andes, Facultad de Ingeniería, Mérida (Venezuela), for his contributions to the curvature-index determination; as well as Peter H. Stone and Charles L. Feldman, both Brigham & Women's Hospital, Cardiovascular Division, Boston MA, and A. Ümit Coşkun, Northeastern University, Mechanical / Industrial / Manufacturing Engineering, Boston MA, for their contributions, the additional in-vivo patient data for the plaque/curvature study, and fruitful discussions on wall shear stresses.

## REFERENCES

1. H. C. Stary, A. B. Chandler, S. Glagov, J. R. Guyton, W. Insull, M. E. Rosenfeld, S. A. Schaffer, C. J. Schwartz, W. D. Wagner, and R. W. Wissler, "A definition of initial, fatty streak, and intermediate lesions of atherosclerosis: A report from the committee on vascular lesions of the council on arteriosclerosis, American Heart Association," *Arteriosclerosis and Thrombosis* **14**, pp. 840–856, May 1994.
2. H. C. Stary, A. B. Chandler, R. E. Dinsmore, V. Fuster, S. Glagov, W. Insull, M. E. Rosenfeld, C. J. Schwartz, W. D. Wagner, and R. W. Wissler, "A definition of advanced types of atherosclerotic lesions and a histological classification of atherosclerosis: A report from the committee on vascular lesions of the council on arteriosclerosis, American Heart Association," *Arteriosclerosis, Thrombosis, and Vascular Biology* **15**, pp. 1512–1531, Sept. 1995.
3. S. Glagov, E. Weisenberg, C. K. Zarins, R. Stankunavicius, and G. J. Kolettis, "Compensatory enlargement of human atherosclerotic coronary arteries," *New England Journal of Medicine* **316**, pp. 1371–1375, May 1987.
4. J. H. C. Reiber, G. Koning, J. Dijkstra, A. Wahle, B. Goedhart, F. H. Sheehan, and M. Sonka, "Angiography and intravascular ultrasound," in *Handbook of Medical Imaging — Volume 2: Medical Image Processing and Analysis*, M. Sonka and J. M. Fitzpatrick, eds., pp. 711–808, SPIE Press, (Bellingham WA), 2000.
5. C. M. Gibson, L. Diaz, K. Kandarpa, F. M. Sacks, R. C. Pasternak, T. Sandor, C. L. Feldman, and P. H. Stone, "Relation of vessel wall shear stress to atherosclerosis progression in human coronary arteries," *Arteriosclerosis and Thrombosis* **13**, pp. 310–315, Feb. 1993.

6. J. J. Wentzel, E. Janssen, J. Vos, J. C. H. Schuurbiers, R. Krams, P. W. Serruys, P. J. de Feyter, and C. J. Slager, "Extension of increased atherosclerotic wall thickness into high shear stress regions is associated with loss of compensatory remodeling," *Circulation* **108**, pp. 17–23, July 2003.
7. A. Wahle, G. P. M. Prause, S. C. DeJong, and M. Sonka, "Geometrically correct 3-D reconstruction of intravascular ultrasound images by fusion with biplane angiography — methods and validation," *IEEE Transactions on Medical Imaging* **18**, pp. 686–699, Aug. 1999.
8. M. E. Olszewski, A. Wahle, R. Medina, S. C. Mitchell, and M. Sonka, "Integrated system for quantitative analysis of coronary plaque via data fusion of biplane angiography and intravascular ultrasound," in *Computer Assisted Radiology and Surgery (CARS 2003)*, H. U. Lemke, K. Inamura, M. W. Vannier, A. G. Farman, K. Doi, and J. H. C. Reiber, eds., *Excerpta Medica International Congress Series* **1256**, pp. 1117–1122, Elsevier, (Amsterdam), 2003.
9. A. Wahle, M. E. Olszewski, and M. Sonka, "Interactive virtual endoscopy in coronary arteries based on multi-modality fusion," *IEEE Transactions on Medical Imaging* **23**, pp. 1391–1403, Nov. 2004.
10. C. B. Burckhardt, "Speckle in ultrasound B-mode scans," *IEEE Transactions on Sonics and Ultrasonics* **25**, pp. 1–6, Jan. 1978.
11. R. F. Wagner, S. W. Smith, J. M. Sandrick, and H. Lopez, "Statistics of speckle in ultrasound B-scans," *IEEE Transactions on Sonics and Ultrasonics* **30**, pp. 156–163, May 1983.
12. M. E. Olszewski, A. Wahle, S. C. Mitchell, and M. Sonka, "Segmentation of intravascular ultrasound images: A machine learning approach mimicking human vision," in *Computer Assisted Radiology and Surgery (CARS 2004)*, H. U. Lemke, M. W. Vannier, K. Inamura, A. G. Farman, K. Doi, and J. H. C. Reiber, eds., *Excerpta Medica International Congress Series* **1268**, pp. 1045–1049, Elsevier, (Amsterdam), 2004.
13. M. E. Olszewski, A. Wahle, S. C. Vigmostad, and M. Sonka, "Multidimensional segmentation of coronary intravascular ultrasound images using knowledge-based methods," in *Medical Imaging 2005: Image Processing*, J. M. Fitzpatrick and J. M. Reinhardt, eds., **5747**, SPIE Proceedings, (Bellingham WA), 2005.
14. R. Medina, A. Wahle, M. E. Olszewski, and M. Sonka, "Three methods for accurate quantification of plaque volume in coronary arteries," *International Journal of Cardiovascular Imaging* **19**, pp. 301–311, Aug. 2003.
15. A. Wahle, R. Medina, K. C. Braddy, J. M. Fox, T. M. H. Brennan, J. J. Lopez, J. D. Rossen, and M. Sonka, "Impact of local vessel curvature on the circumferential plaque distribution in coronary arteries," in *Medical Imaging 2003: Physiology and Function: Methods, Systems, and Applications*, A. V. Clough and A. A. Amini, eds., **5031**, pp. 204–213, SPIE Proceedings, (Bellingham WA), 2003.
16. A. Wahle, M. E. Olszewski, S. C. Vigmostad, R. Medina, A. Ü. Coşkun, C. L. Feldman, P. H. Stone, K. C. Braddy, T. M. H. Brennan, J. D. Rossen, K. B. Chandran, and M. Sonka, "Quantitative analysis of circumferential plaque distribution in human coronary arteries in relation to local vessel curvature," in *Proc. 2004 IEEE International Symposium on Biomedical Imaging*, pp. 531–534, IEEE Press, (Piscataway NJ), 2004.
17. Y. G. Lai and A. J. Przekwas, "A finite-volume method for fluid flow simulations with moving boundaries," *Computational Fluid Dynamics* **2**, pp. 19–40, 1994.
18. S. D. Ramaswamy, S. C. Vigmostad, A. Wahle, Y. G. Lai, M. E. Olszewski, K. C. Braddy, T. M. H. Brennan, J. D. Rossen, M. Sonka, and K. B. Chandran, "Fluid dynamic analysis in a human left anterior descending coronary artery with arterial motion," *Annals of Biomedical Engineering* **32**, Dec. 2004.